Optics and Lasers in Engineering 50 (2012) 8–17

Contents lists available at ScienceDirect

Optics and Lasers in Engineering

journal homepage: www.elsevier.com/locate/optlaseng

# A comparison of three quantitative schlieren techniques

Michael J. Hargather *, Gary S. Settles

*Gas Dynamics Laboratory, Pennsylvania State University, Department of Mechanical and Nuclear Engineering, 301D Reber Building, University Park, PA 16802, USA*

ARTICLE INFO

Available online 11 June 2011

*Keywords:*
Quantitative schlieren
Background-oriented schlieren
Density measurement
Flow visualization

ABSTRACT

We compare the results of three quantitative schlieren techniques applied to the measurement and visualization of a two-dimensional laminar free-convection boundary layer. The techniques applied are Schardin's "calibrated" schlieren technique, in which a weak lens in the field-of-view provides a calibration of light deflection angle to facilitate quantitative measurements, "rainbow schlieren", in which the magnitude of schlieren deflection is coded by hue in the image, and "background-oriented schlieren" (BOS), in which quantitative schlieren-like results are had from measuring the distortion of a background pattern using digital-image-correlation software. In each case computers and software are applied to process the data, thus streamlining and modernizing the quantitative application of schlieren optics. (BOS, in particular, is only possible with digital-image-correlation software.) Very good results are had with the lens-calibrated standard schlieren method in the flow tested here. BOS likewise produces good results and requires less expensive apparatus than the other methods, but lacks the simplification of parallel light that they feature. Rainbow schlieren suffers some unique drawbacks, including the production of the required rainbow cutoff filter, and provides little significant benefit over the calibrated schlieren technique.



## 1. Introduction

Quantitative schlieren techniques are those intended to measure refractive-index-distributions and related quantities in transparent media [1]. Since the schlieren effect is due to refraction, it was suggested in the 1930s by Schmidt [2] and Schardin [3,4] that it be used to measure refraction, from which density and temperature are readily extracted in simple fluid flows. Since that time many different quantitative schlieren methods have been published.

Quantitative schlieren was, however, somewhat ahead of its time in that pre-computer era. Since schlieren results required densitometry and integration by hand, the more-direct interferometry approach was preferred. Computers can now, however, conveniently manage all data handling and processing chores for quantitative schlieren (and interferometry). The overall result is that journal publications on quantitative schlieren rose steadily from a handful in the 1940s to more than 70 during 2000–2010: not a widely used scientific tool, but also not a negligible one.

Given the many quantitative schlieren methods proposed in the literature, potential users need to know relative performance metrics in order to choose which method to use. Studies that apply several such methods to the same flow are very useful for this purpose, but are rare. There has been one such study published in the past decade: Elsinga et al. [5]. These authors did an elaborate comparison of a quantitative color schlieren method with background-oriented schlieren (BOS) for the investigation of density fields in a supersonic wind tunnel. Both methods produced results within about 2% of the known theoretical curves, but BOS suffered in this comparison due to limited spatial resolution because the wind-tunnel test section was not sharply focused. We believe further comparison is warranted, especially between traditional schlieren methods and the new non-traditional BOS technique.

The BOS technique was introduced almost simultaneously by Meier [6] and by Dalziel et al. who called it "synthetic schlieren" [7]. A better name for it would be "synthetic background-distortion schlieren," but the BOS acronym has now firmly taken hold. In its simplest form it consists merely of a randomly speckled background and a camera. High-resolution images are made of the background by the camera with and without refractive disturbances between the two. Post-processing of image pairs using software then reveals small distortions of the background due to refraction, from which schlieren-like images can be derived.

These authors, however, were not the first to discover the background-distortion effect of transparent refractive media, which was published by Hooke [8] and more recently by Schardin [4], who established this as a rudimentary schlieren technique. Neither the camera nor the background is essentially new in BOS, but the addition of digital cameras and image processing makes this a new and valuable flow visualization technique [9–18].

* Corresponding author.
*E-mail address:* mjh340@psu.edu (M.J. Hargather).

0143-8166/$ - see front matter © 2011 Elsevier Ltd. All rights reserved.
doi:10.1016/j.optlaseng.2011.05.012

The prolific Schardin [4] also first described the quantitative use of color in schlieren imaging, including the use of a prism near the light source to produce spectrum colors and later the replacement of the knife-edge by a lattice filter (*Gitterblende*) composed of transparent color bands and opaque bars. The quantitative use of these techniques provided schlieren images in color, where the various colors identified the magnitudes of the light refraction. However, many applications of these techniques remained qualitative due to the workload involved in handling and integrating the experimental data.

Howes [19,20] introduced the term "rainbow schlieren" to describe color schlieren images created by replacing the knife-edge with a color transparency having a continuous spectrum rather than discrete bands as used by Schardin. Greenburg et al. [21] built upon this to pioneer the digitization of the rainbow-schlieren image and the use of digital colorimetry to automatically extract quantitative refraction data from it. This trend toward computer-automated data acquisition and reduction was later taken up by Agrawal et al. who published prolifically on quantitative rainbow-schlieren imaging in planar and axisymmetric flows, unsteady flows, and combustion experiments, e.g. [15,22–29]. Rainbow schlieren has become the leader of quantitative schlieren methods in the literature today because it is simple, robust, useful, well-developed, and highly automated.

The third method of interest is photometric quantification of the gray scale in an ordinary schlieren image. This has also been done before on a number of occasions [1], but we revisit it here for its simplicity and ease of use. This technique is quantified here using a weak positive lens in the schlieren image as a "calibration Schliere," as suggested by Schardin [3,4]. Though it has seen limited use, this approach to quantitative schlieren measurements has some important advantages including simplicity: typically no modifications are required to an existing schlieren optical system.

In order to compare these three quantitative optical approaches the simple refractive two-dimensional steady flow-field of the free-convection laminar boundary layer on a heated vertical flat plate is used, as was done in [30], where a grid-cutoff schlieren method (focal filament) has been employed. This classical heat transfer test case avoids problems of glass windows and wind-tunnel vibration that have clouded other quantitative schlieren studies. Further, the theoretical temperature profile of the boundary layer is well-known [31].

## 2. Background

### 2.1. Laminar free-convection flat plate boundary layer

The laminar free-convection flat plate boundary layer was solved theoretically by Ostrach using a similarity solution to relate the non-dimensional temperature and velocity profiles to a length parameter $\eta$ [31]. The similarity parameter $\eta$ combines the distance from the plate leading edge, $x$, and the perpendicular distance from the plate surface, $y$:

$$\eta = \left(\frac{Gr_x}{4}\right)^{1/4}\frac{y}{x} \tag{1}$$

Where the Grashof number, $Gr$, at a distance $x$ from the leading edge of a flat plate is defined as

$$Gr = \frac{g\beta(T_p - T_\infty)x^3}{\nu^2} \tag{2}$$

In which $g$ is the gravitational acceleration, $T_p$ is the plate surface temperature, $T_\infty$ is the free-stream air temperature, $\nu$ is the free-stream air kinematic viscosity, and $\beta$ is the coefficient of thermal expansion.

The boundary layer temperature distribution, $T$, is given by the function $H$:

$$H(\eta) = \frac{T - T_\infty}{T_p - T_\infty} \tag{3}$$

This similarity solution is solved numerically and tabulated by Ostrach for varying Prandtl number, $Pr$ [31], which is used here with $Pr = 0.72$ to define a theoretical temperature distribution around the flat plate in air. The flat plate used here has dimensions of $0.152 \times 0.013 \times 0.152$ m, measured in the $x$ (length along plate in gravity direction), $y$ (width across schlieren light beam), and $z$ (length along optical axis) directions, respectively. The plate was heated electrically by a resistive heater on the side opposite the measurement face. The plate was heated until it reached steady state, determined when its surface temperature did not change for 10 min. The surface temperature at multiple locations on the plate was measured using a thermocouple, and was found to vary a maximum of $\pm 1$ K. The steady-state plate surface temperature was $T_p = 333.0$ K with $T_\infty = 293.7$ K.

### 2.2. Light refraction principles

Light rays passing through a transparent medium of varying refractive index are bent based on the spatial refractive-index gradients [1]. Fig. 1 schematically shows a light ray being refracted due to the hot thermal boundary layer surrounding a flat plate of length $Z$. A light ray, traveling in the $z$-direction, is refracted through an angle $\varepsilon_y$ due to the refractive-index gradient in the $y$-direction. For a two-dimensional schliere of extent $Z$ this is

$$\varepsilon_y = \frac{1}{n}\int \frac{\partial n}{\partial y}\partial z = \frac{Z}{n_\infty}\frac{\partial n}{\partial y} \tag{4}$$

The refractive index, $n$, of a gas is related to the density of the gas, $\rho$, through the Gladstone–Dale relation [1], which is used here with the Gladstone–Dale constant for air, $\kappa = 2.23 \times 10^{-4}$ m$^3$/kg:

$$n = \kappa\rho + 1 \tag{5}$$

The density-gradient field within a gas can thus be directly quantified by measuring the refractive-index gradient field, which is obtained through each of the three experimental techniques presented here. The refractive-index gradients are "calibrated" here through the use of a weak simple positive lens as shown by Schardin [4] (other calibration objects are also presented by Schardin).

### 2.3. Calibration lens

A simple positive lens, with incoming parallel light, will focus all of the light rays to a point, as shown schematically in Fig. 2. Each light ray that passes through the lens at a different radial location $r$ will be refracted through a different angle, from zero at the center of the lens to a maximum refraction angle $\varepsilon_R$ at the radius of the lens, $R$.

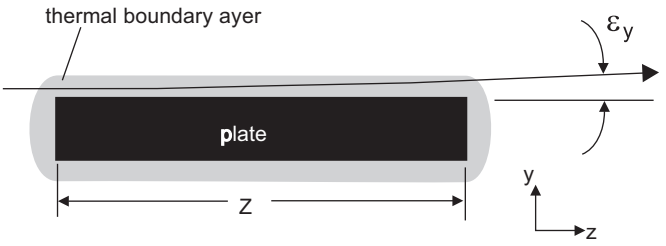


**Fig. 1.** The thermal boundary layer on a heated plate of length $Z$ refracts a light ray through an angle $\varepsilon_y$. For purposes of quantitative analysis, the entire ray deflection $\varepsilon_y$ is assumed to occur at once in the center of the present two-dimensional flow, i.e. at the center of the plate.

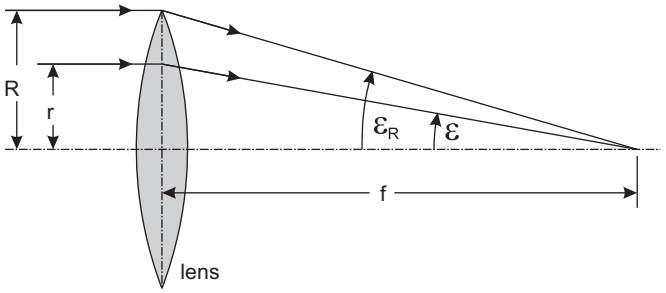


**Fig. 2.** Schematic of a simple lens used as a calibration object for quantitative schlieren visualization. In practice, long-focal-length positive meniscus lenses serve this purpose well. Spherical and chromatic aberrations are negligible for such lenses.

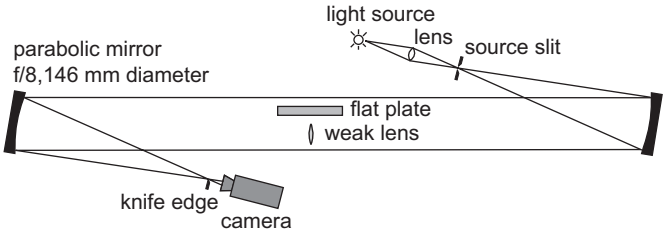


**Fig. 3.** Schematic of the parallel-light z-type schlieren system used for calibrated schlieren and rainbow schlieren.

Within a schlieren system a lens calibration can be used, and is used here, to provide a quantifiable relationship between refraction angle and image pixel intensity or color. A light ray which passes through an arbitrary location on the lens, $r$, will be refracted through an angle $\varepsilon$:

$$\frac{r}{f} = \tan\varepsilon \approx \varepsilon \tag{6}$$

The calibration lens must be a "weak" lens with a long-focal-length, such that it produces refraction angles within the range of interest for the schlieren disturbances to be visualized. For the present work a lens of $R=25.4$ mm and $f=10$ m from CVI Laser, LLC, is used (part number: PLCX-25.4-5151.0-C, cost: about $90), which allows the quantification of refraction angles up to 524 arcseconds. A weak lens also results in $R \ll f$ such that the small angle approximation in Eq. (6) is justified.

## 3. Optical techniques

Each of the three different quantitative methods that are used here can be categorized by whether the light that passes through the measurement region is parallel (calibrated schlieren and rainbow schlieren) or divergent (background-oriented schlieren). The methods by which the refraction is visualized in each technique are different, but the basic principles of light refraction are the same in each application.

### 3.1. Parallel-light schlieren optics

A z-type parallel-light schlieren system is used here and is shown schematically in Fig. 3. This system is used for both calibrated schlieren and rainbow schlieren, the only difference being in the nature of the cutoff placed in the knife-edge position. The camera should be focused sharply at the location of the test object [1]. Here the camera is focused on the calibration lens, which is positioned at the centerline of the flat plate. A Nikon D80 digital SLR camera was used to record all present images. In principle a broad range of digital cameras might be used, but a camera with high pixel resolution and a large pixel-bit depth is desired to maximize spatial resolution and the ability to resolve a greater range of pixel intensities, and thus refraction angles.

#### 3.1.1. Calibrated schlieren

The calibrated schlieren system uses a white light-emitting diode (LED) as the light source with a source slit of about $1 \times 1$ mm. A LED is used here because it provides uniform illumination across the entire field-of-view, as observed in Fig. 4. For quantitative schlieren the background illumination must be relatively constant because all refraction angles are measured relative to the background pixel intensity.

The knife-edge cutoff is placed vertically for the present visualizations, thus resulting in the visualization of horizontal refractive-index gradients in the test region. Light that is refracted horizontally moves onto or off of the knife-edge, resulting in a darker or lighter region in the image, respectively. A fraction of the unrefracted schlieren beam is "cut off" by the knife-edge, resulting in the gray pixel-intensity level of the background [1]. Any refractive disturbance increases or decreases this background pixel intensity, thus the presence of a refractive disturbance in the image must be measured relative to the grayscale intensity of the image background, where no refractive disturbances occur.

The calibration lens refracts the parallel light and causes it to be focused to a location beyond the knife-edge position. As this

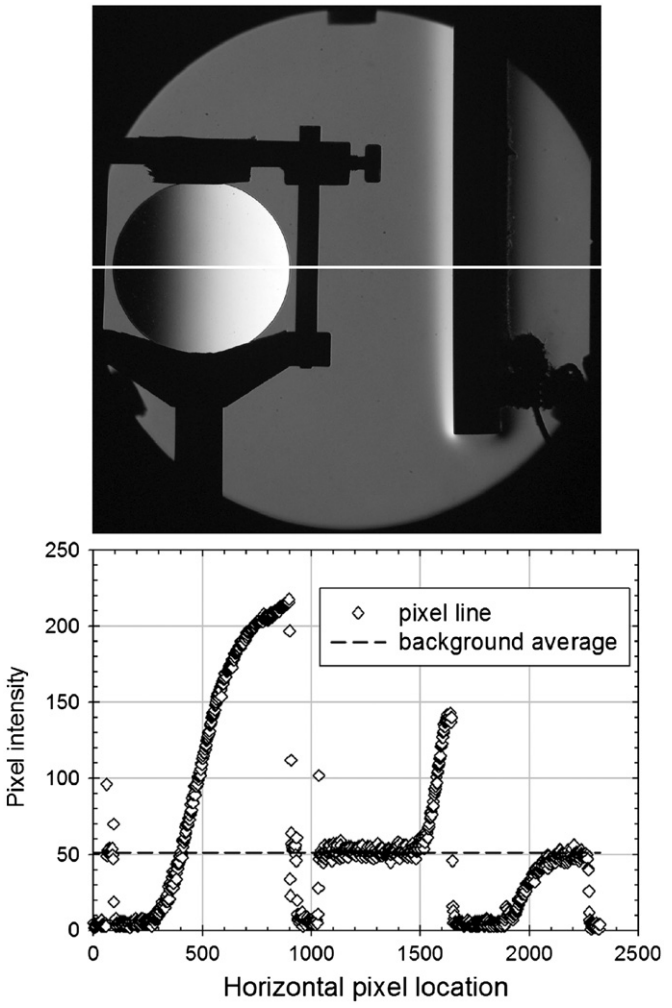


**Fig. 4.** A typical schlieren image, recorded with a vertical graded-filter cutoff, showing the calibration lens and the flat plate as well as a plot of measured pixel intensity across the image at the location indicated by the white line.

light passes the knife-edge it is also "cutoff" due to the refraction angle within the lens, resulting in the intensity gradient observed in Figs. 4 and 5. The intensity gradient within the lens image is observed as a purely horizontal gradient because a vertical knife-edge cutoff is used, thus revealing only the horizontal refractions of the lens. Each grayscale pixel intensity in the lens image occurs at a specific horizontal position, which can be quantified to a horizontal refraction angle using Eq. (6).

The calibration process begins by identifying the average background pixel intensity of the image. The same intensity value is then identified in the calibration lens image, as seen in Fig. 4. The distance of this point from the center of the lens, measured along the horizontal diameter for vertical knife-edge cutoff, is defined as $r_0$ because it represents the pixel-intensity value corresponding to no refraction in the image, and it is the baseline for all other measurements. The point $r_0$ on the lens refracts light through an angle $\varepsilon_0$ as defined by Fig. 2 and Eq. (6). This calibration lens caused negligible light losses, so no correction was applied as discussed by Schardin [4].

The refraction angle at any point in the schlieren image is now quantified by first identifying the location within the calibration lens image that has the same pixel intensity as the point of interest. This point in the lens image has a distance from the lens center of $r$ and refracts light through an angle $\varepsilon$. The refraction at the corresponding point in the schlieren image, $\varepsilon_{image}$, is equal to the relative refraction angle between the lens positions $r$ and $r_0$, which after applying Eq. (6) and the small angle approximation, becomes:

$$\varepsilon_{image} = \varepsilon - \varepsilon_0 = \frac{1}{f}(r - r_0) \tag{7}$$

Once $\varepsilon_{image}$ is obtained for a point in the image, Eqs. (4) and (5) are used to determine the air density at that point. The air temperature profile is obtained by applying an equation of state and assuming a pressure value or distribution as appropriate. Here the air was assumed to behave as an ideal gas and the pressure was assumed not to vary from one atmosphere across the thermal boundary layer.

One critical aspect of this quantification process is that each location within the calibration lens image has a unique pixel-intensity value and that corresponding pixel-intensity values are also observed in the schlieren image. The pixel-intensity-value range observable in the calibration lens represents the measuring *range* of the schlieren system, i.e. the range of light refraction angles that are observable. This range of observable refractions must be balanced with the *sensitivity* of the schlieren system, i.e. the minimum refraction angle that can be detected. The inherent balance between sensitivity and range is observed in all schlieren systems [1] and is illustrated in Fig. 5.

In Fig. 5, two schlieren cutoffs are examined: a knife-edge and a graded filter. The knife-edge cutoff is typical for schlieren visualization and provides the greatest sensitivity (ability to detect small refraction angles) but the lowest measuring range (breadth of measurable refraction angles). The high sensitivity of the knife-edge cutoff is shown in Fig. 5c by the large slope of the pixel-intensity curve. The limited range is observed in the regions beyond +100 and −200 pixels from the lens center, where the pixel-intensity values become constant. The graded filter [1], which is made by a photographic process to produce a near-linear variation of transparency over a small distance in place of a sharp edge, yields a wider measuring range of the schlieren image but reduced sensitivity. The present graded filter has a transparent-to-opaque gradient extending over a distance of approximately 2 mm, but other graded filters of various widths can be used to tune the range and sensitivity of a given schlieren system [1].

The knife-edge and graded-filter cutoffs result in differences in the appearance of the heated-plate thermal boundary layer used here, as shown in Fig. 6. The knife-edge-schlieren image in Fig. 6a qualitatively appears dark, but the graph of pixel intensity reveals that the image appropriately maximizes the pixel-intensity values available with the present measurement range. The graded-filter-schlieren image in Fig. 6b is qualitatively better for observing the schlieren effect, but quantitatively yields a narrower range of pixel intensities for this measurement. The graded-filter image will thus have greater error in the refraction-angle measurement because of its limited range of pixel intensities used to record the image.

A camera with a greater pixel-intensity range, or bit depth, also improves the sensitivity and accuracy of the measurement, and thus is preferred. Note also that image processing such as contrast stretching does not yield more quantitative schlieren sensitivity, it merely stretches the original data and improves the qualitative appreciation of the schlieren image. The latter is

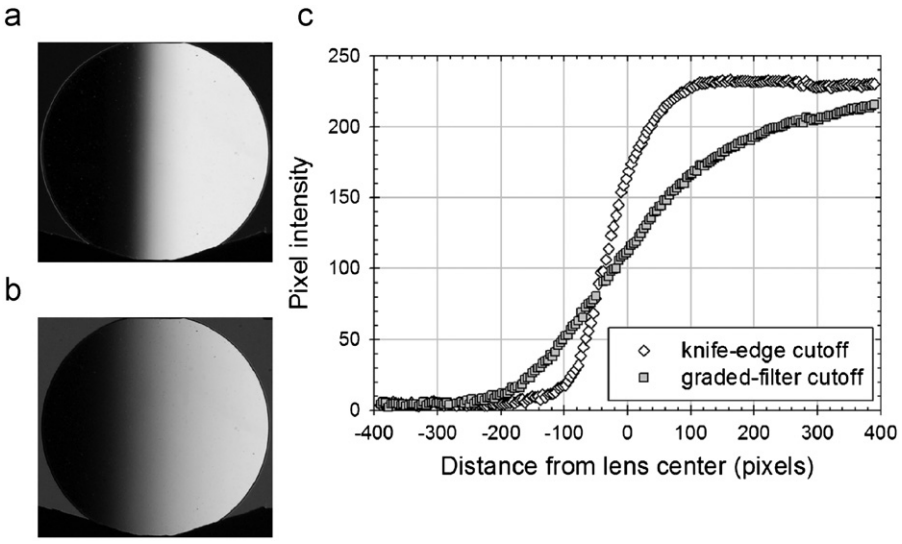


**Fig. 5.** Schlieren visualization requires an appropriate balance between high sensitivity and a large measurement range. (a) A knife-edge cutoff provides the greatest sensitivity, but with a limited range. (b) A graded-filter cutoff allows a larger measurement range at the expense of sensitivity. (c) The sensitivity of a schlieren cutoff is observed as the maximum slope of the pixel-intensity curve in the calibration lens image, while the measurement range is defined as the horizontal distance over which the observed pixel intensity varies.

discussed at length in [1], where examples are shown of schlieren images containing information not available to the human eye without image processing. Image-processing a quantitative schlieren image and its calibration, however, would have no effect on the final data unless information was lost in the process.

### 3.1.2. Rainbow schlieren

Rainbow schlieren provides a quantification of light refraction through the use of a color cutoff filter in place of a knife-edge [20,21,25,28]. This "rainbow" cutoff is placed at the knife-edge position in a schlieren system, as diagrammed in Fig. 3, so that the light passing through it takes on the hue of the location on the filter that it passes through. The rainbow cutoff used for the present experiments is shown in Fig. 7a, and is positioned so that the color bands are vertical, resulting in the color-coding of horizontal refractions.

To maximize the sensitivity of a rainbow schlieren cutoff, the color should vary continuously with distance so that the refracted light passes through a unique color based on its refraction angle. This further requires that the schlieren illumination source-slit size is narrow, so that all of the background illumination passes through a single color. In the current setup the light source slit is $2 \times 10^{-5}$ m wide, with a vertical extent of approximately 3 mm (the vertical extent of the schlieren source is relatively unimportant in the present vertical-cutoff configuration). The LED light source used for calibrated schlieren could not be focused sharply enough for this narrow source-slit size, so a 100 W xenon arc lamp was used instead. Increasing the source-slit width reduces the sensitivity of the rainbow-schlieren method in a manner similar to that of changing from a knife-edge to a graded filter.

The measurement range of a rainbow-schlieren cutoff is determined only by the width of the color filter used. The size of the source slit does not affect the measurement range of the system.

The calibration for converting an imaged color to a refraction angle is obtained here with the calibration lens as previously described in Section 3.1.1. Instead of a grayscale pixel-intensity

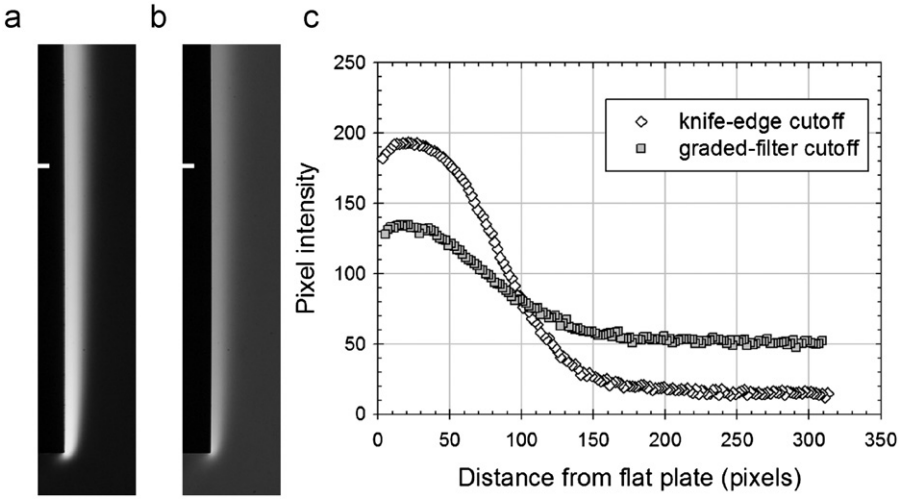


**Fig. 6.** The thermal boundary layer on the heated flat plate is measured using (a) knife-edge and (b) graded-filter schlieren cutoffs. (c) The pixel intensity as a function of distance from the plate surface is shown for the marked plate location in images (a) and (b).

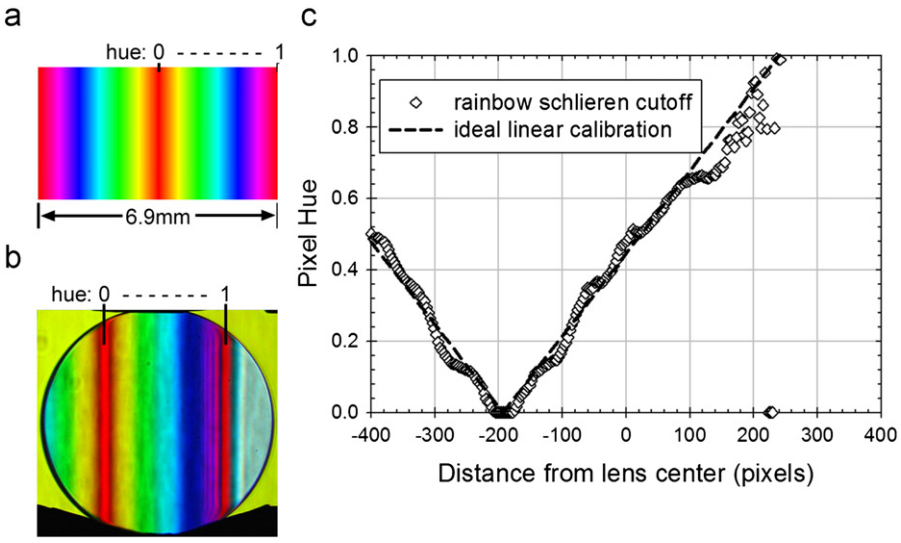


**Fig. 7.** Rainbow schlieren uses color to quantify refraction angles. (a) The present rainbow cutoff has a linearly varying hue from 0 to 1 and is symmetric about hue = 0 (red). (b) The calibration lens is used to relate hue to a refraction angle. A yellow background hue can be observed around the lens, indicating that the unrefracted source illumination is passing through the yellow hue band in this particular example. (c) The pixel hue versus lens position calibration showing the measured cutoff hue is shown along with the ideal linear relationship for reference. (For interpretation of the references to color in this figure legend, the reader is referred to the web version of this article.)

calibration versus position in the lens image, the rainbow-schlieren calibration relates a hue to each location in the lens image (Fig. 7b and c). Again, refractions are measured relative to the background hue of the image, which is yellow in the particular example shown in Fig. 7b. The calibration can also be performed by traversing the rainbow cutoff horizontally in the cutoff plane and recording the background image hue, e.g. [28]. A specific hue in the image can then be directly related to a horizontal displacement through which the light ray was refracted, measured in the cutoff plane as the distance between the background hue and the observed hue. Both calibration approaches were experimentally tested in our work, but the use of the calibration lens was found to be simpler and more precise, and is thus the only method presented here.

The color images recorded by the camera are converted from the red–blue–green (RGB) color scale to the hue-saturation-intensity (HSI) color scale [32]. This color scale is used because each color is uniquely and numerically identified as a hue, independent of its dilution by white light (saturation) or its brightness (intensity).

The rainbow filter master, shown in Fig. 7a, was created using Adobe Photoshop with 360 vertical bands of linearly varying hue from 0 to 1, beginning with red (hue=0) through yellow ($\sim$0.2), green ($\sim$0.4), blue ($\sim$0.6), purple ($\sim$0.8), and back to red (hue=1). The filter itself was produced through a photographic film exposure and development process to obtain a transparent slide. After smoothing, the master image was displayed full-size on a flat-screen computer monitor and photographed onto Fujichrome ISO 100 transparency film using a vintage Minolta X-700 SLR camera with a 50 mm fixed lens and a 1-sec exposure. The film was E-6 processed to yield a transparency, Fig. 7b, in which the entire hue range from 0 to 1 occurred over a width of 3.45 mm. This transparency was used directly as a schlieren cutoff to yield the calibration shown in Fig. 7c. Greenberg et al. [21] have described the nonlinearities that arise in this process and an iterative means to correct them. However, we judged the calibration of Fig. 7c to be adequate for present purposes without correction. Gamma Tech (http://www.gammatech.com/) produces transparencies directly from digital files, which should yield better results than the photographic process used here. Several modern digital printing techniques were also attempted to produce the cutoff filters, but these were not able to reproduce the color bands with sufficient resolution and transparency.

### 3.2. Diverging-light background-oriented schlieren (BOS)

The BOS technique is distinct from the previous two techniques in that the light rays passing through the test region are diverging (viewed from the camera perspective) and that computer processing is required to obtain schlieren-like images.

The typical BOS experimental setup is equivalent to Schardin's schlieren method #1 [4] and is illustrated in Fig. 8. The BOS background is composed of unique and randomly distributed features [33] which are distorted by the presence of refractive disturbances between the camera and the background [6]. The BOS visualization requires two images, one with no flow disturbances and one with the flow disturbance to be studied, which are image-processed to identify locations where the background pattern is observed to "shift" location. This "pixel shift" is quantified using digital-image-correlation software that identifies unique locations within the no-flow image and then determines their location in the flow-distorted image. Here, commercial Vic-2D software from Correlated Solutions, Inc. is used to process the images, although in principle any digital-image-correlation software or cross-correlation algorithm could be used [34].

The sensitivity of a BOS system is a function of the optical geometry shown in Fig. 8 and the camera characteristics. In general,

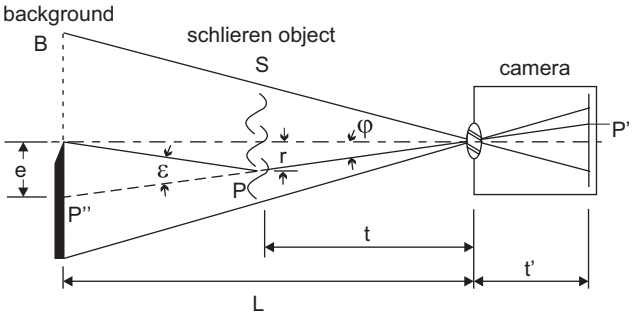


**Fig. 8.** Schematic of Schardin's schlieren method #1, the typical optical arrangement for BOS imaging. For simplicity a single light-dark boundary is shown as the background, but in practice a random pattern composed of many light-dark boundaries is used. The background used in the present experimental results was composed of randomly distributed black squares ($0.7 \times 0.7$ mm) on a white background of $0.2 \times 0.2$ m [33].

the ratio of camera-to-schlieren-object distance $t$ to camera-to-background distance $L$ should be minimized and $L$ should be maximized for the greatest sensitivity. This is constrained, however, by depth-of-field, since maintaining both the background and schlieren object in reasonable focus is important for the success of the BOS technique. The camera must be sharply focused on the BOS background in order to accurately measure pixel shifts. At the same time the schlieren object must remain in focus for good schlieren imaging, and in order to measure successfully near solid surfaces (e.g. the present flat plate surface), which will otherwise become blurred and obscure the image of the background. Typically the required sensitivity is established by choosing a suitable distance $L-t$ within the constraints of a given experimental setup (i.e. room size), and then choosing $t$ for acceptable depth-of-field. Ideally the schlieren object will be halfway between the camera and the background ($t/L=0.5$) for maximum sensitivity, but this requires a large depth-of-field that is not practically attainable within the confines of many experimental setups. The present experimental work presents results for $t/L=0.75$ and 0.875.

The camera used for recording BOS images also influences the sensitivity of the system. For maximum sensitivity a long-focal-length lens and high pixel resolution is desired. The current measurements used a 200 mm lens on the Nikon D80 SLR, which has 10.2 megapixel resolution. The lens was stopped down to $f/22$ to maximize the depth-of-field of the image.

BOS sensitivity is also dependent on the image-correlation algorithm used and its ability to accurately measure pixel shifts. Many digital-image-correlation algorithms include sub-pixel resolution capabilities, which are advantageous here. Sub-pixel resolution, however, is typically only accurate to $\pm 0.1$ pixels.

BOS is unique in that the calibration lens does not need to be used to perform the refraction-angle-to-pixel-displacement calibration; it is used here only for completeness and for comparison between techniques. In BOS the pixel shift, when measured in the physical distance scale of the background, is directly related to the refraction angle through trigonometry:

$$\frac{\text{pixel shift}}{L-t} = \tan\varepsilon \approx \varepsilon \tag{8}$$

The measured horizontal pixel shifts in the calibration lens image, observed at two different ratios of $t/L$, are shown in Fig. 9. The graph in Fig. 9c shows that increased sensitivity is obtained with a decreasing ratio of $t/L$ (i.e. the subject moves closer to the camera and away from the background). The graph also shows that the sensitivity for varying $L$ at constant $t/L$ does not change, which appears contrary to the previous statement of increased sensitivity with increased $L$. The results shown here for $L=2.54$

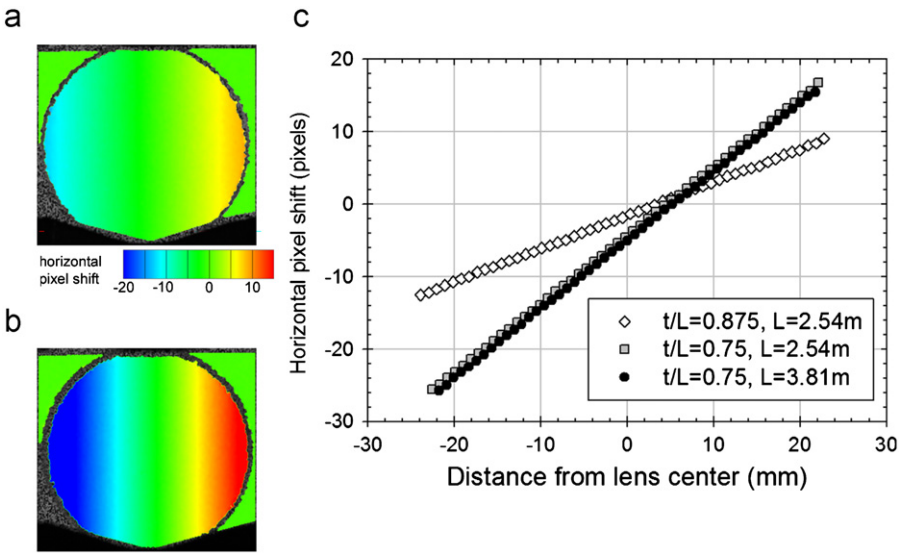


**Fig. 9.** The sensitivity of a BOS system is demonstrated with the calibration lens. The measured horizontal pixel shift in the lens image is shown for $L=2.54$ m with (a) $t/L=0.875$ and (b) $t/L=0.75$. (c) The measured pixel shift as a function of location in the lens image for varying BOS geometry. The sensitivity of a BOS system increases with decreasing $t/L$.

and 3.81 m use the same camera and 200 mm lens, thus the sensitivity gained through increasing the distance $L$ is lost due to an effectively reduced pixel resolution because of the increased distance $L$. Any sensitivity increase with increasing $L$ is dependent upon maintaining pixel resolution, which would require increasing the zoom of the camera lens or increasing the camera pixel resolution to regain the same pixel-width-to-distance correspondence in the BOS background plane.

One complication of BOS imaging is that the divergent light ray geometry requires a more-complex pixel-to-length calibration of the image than before. With the camera focused on the BOS background, the pixel-to-length calibration is performed in the plane of the background. The observed pixel shifts are also calculated in the plane of the background. The actual refraction occurs at the schlieren-object position, which has a foreshortened length due to the divergent light. Thus the measured length in the background plane $B$ must be converted to a length in the object plane $S$ using trigonometry and Fig. 8. The background pixel shift does not have to be corrected because it occurs on the background itself and therefore should be measured using a background calibration length.

The divergent light also requires a precise alignment of the BOS optical components. For accurate visualization of refractions near a flat surface (e.g. the flat plate used here), the flat surface where measurements are to be taken must lie along the camera lens centerline, which should then be perpendicular to the BOS background. Refractions near a flat surface can only be measured if the flat surface is parallel with one of the divergent light rays that can be traced through the camera lens. Measurements using BOS cannot therefore be made simultaneously on two parallel surfaces (e.g. top and bottom walls of a wind-tunnel test section) without sacrificing measurement resolution near one or both surfaces.

## 4. Experimental measurement of free-convection thermal boundary layer

The thermal boundary layer on the flat plate was first examined to determine whether the streamwise temperature profiles along the plate accurately scale according to the theoretical solution. Three $x$ locations along the plate were identified for this analysis, which was performed using knife-edge-cutoff calibrated schlieren, as shown in Fig. 10. The deflections measured in the schlieren image of Fig. 10 were converted to refractive-index gradients using Eq. (4). The refractive-index gradient field was then integrated using a simple first-order integration scheme starting from a point in the "background" of the image where the refractive index was calculated from the free-stream temperature. Ultimately the refractive-index field was converted to a temperature field through Eq. (5) and the ideal gas law. Distance and temperature were then non-dimensionalized using Eqs. (1) and (3), respectively.

The resulting non-dimensional temperature as a function of non-dimensional distance is plotted in Fig. 10b for each position along the plate.

Good agreement of these data indicates that the measurement regions selected are independent of any leading edge effects, and that the width of the plate is sufficient to avoid three-dimensional end effects. The agreement also demonstrates that the two-dimensional schlieren disturbance assumption made in Eq. (4) is appropriate and that the procedure for obtaining the temperature profile is accurate.

The error in the measurements shown in Fig. 10, $\pm 0.03$ or $\pm 3\%$ of the overall temperature difference, represents the accumulation of errors due to the measurement of the plate surface temperature, the free-stream temperature, the pixel-distance calibration within the image, the identification of the flat plate surface in the image, and the variation of pixel-intensity values in the undisturbed regions of the schlieren image.

Each technique as described in Section 3 was next applied to measuring the thermal boundary layer at the location $x=79$ mm on the flat plate. The temperature distribution as a function of distance from the plate surface was calculated from the refraction data obtained from the schlieren images. The final results of these measurements of the temperature distribution are presented in Fig. 11.

The measured temperature profiles are nearly indistinguishable among the different measurement techniques, and are within the error limits ($\pm 3\%$) of each other and the theoretical profile. This graph shows that each of the techniques considered here is capable of measuring this temperature distribution accurately in this simple flow.

The conversion from schlieren image output, $\varepsilon_y$, to temperature, however, involves the integration of the refractive-index gradient field. This integration can effectively hide small

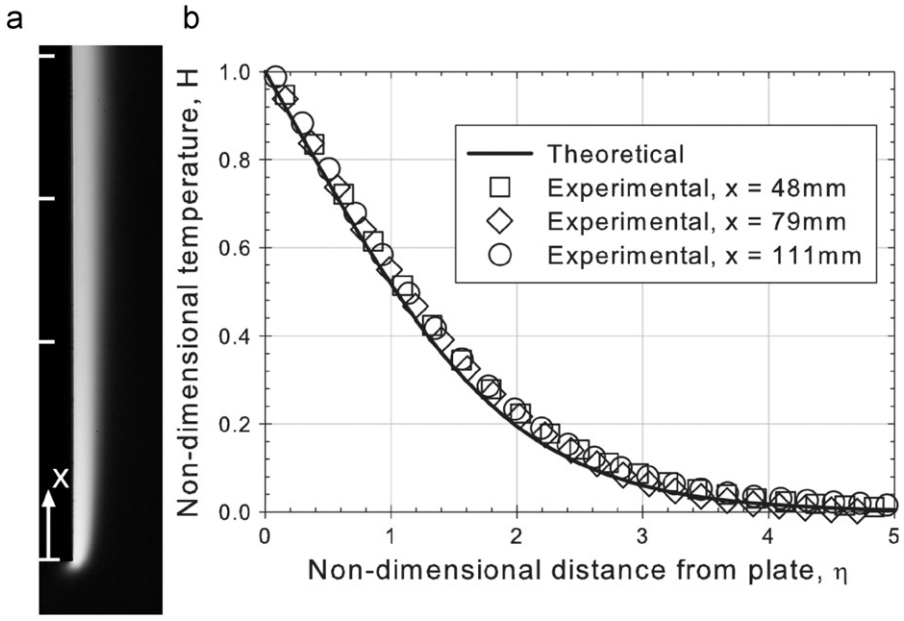


**Fig. 10.** (a) The knife-edge-cutoff calibrated schlieren technique is used to measure the refractive-index gradient field at three different $x$ locations along the flat plate (of length 0.152 m). (b) The profiles of non-dimensional temperature versus non-dimensional distance from the plate are shown at each of the three distances along the plate, and are all found to be in good agreement with the theoretical profile. The size of the symbols in the graph represents the estimated error in the measurement.

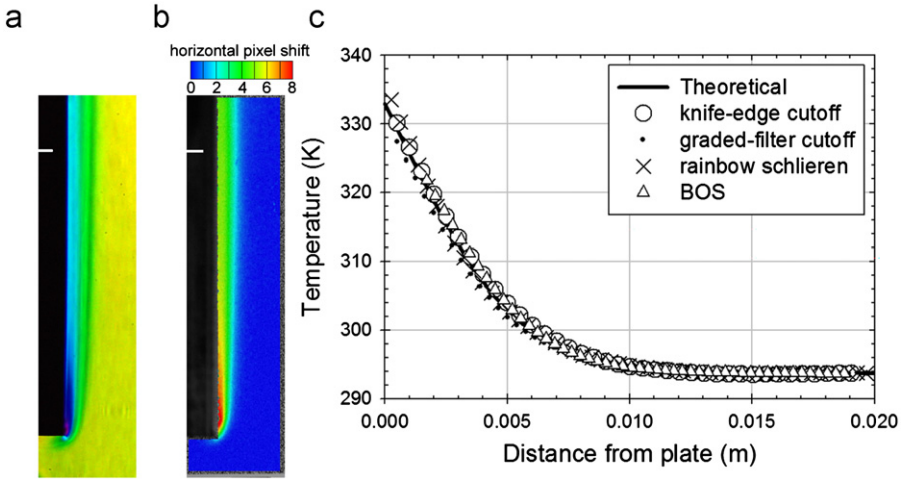


**Fig. 11.** (a) Rainbow-schlieren image of the heated plate. (b) BOS image of the heated plate with $t/L$=0.75 and $L$ = 2.54 m. (c) Measured temperature profile of the boundary layer on the heated flat plate for each of the three quantitative schlieren methods, compared to the theoretical profile. The size of the round symbol for the knife-edge cutoff case is representative of the estimated error in each measurement. The calibration for (a) was shown previously in Fig. 7 and the calibration for (b) was shown in Fig. 9.

differences in the measured deflection angle. Accordingly, Fig. 12 shows the raw measured refraction angle as a function of distance from the plate surface for each of the quantitative techniques.

By examining Fig. 12 it can be seen that each of the techniques accurately measures the refraction angle as a function of distance with reasonable common agreement and good correspondence to the theoretical profile.

The rainbow-schlieren results have the largest errors from the theoretical profile, especially near the plate surface. This is likely due to diffraction by the rainbow filter of light already diffracted once by the plate. The small slit width and narrow color bands used in the rainbow-schlieren technique cause more-significant diffraction effects than are observed in the other parallel-light schlieren systems. The rainbow-schlieren results are also more error-prone due to the photographically developed color cutoff and its calibration problems, which results in more error in determining the hue distribution in the calibration lens image and the schlieren image. Improving the cutoff hue calibration through an iterative process of creating and developing new cutoffs could be performed, but the results are not expected to surpass the calibrated schlieren results.

The BOS results are nearly as good as the knife-edge schlieren results, with the exception of the inability to measure near the plate surface. The parallel light and sharp focus on the plate achieved with the knife-edge schlieren optics images the measurement of refraction angle to within a few pixels of the plate surface (1 pixel $\approx$0.06 mm in the present parallel-light schlieren images). By comparison the diverging light and blur of the plate in the BOS images limits the measurement to a larger distance from the plate surface (1 pixel $\approx$0.10 mm in the background of the BOS images).

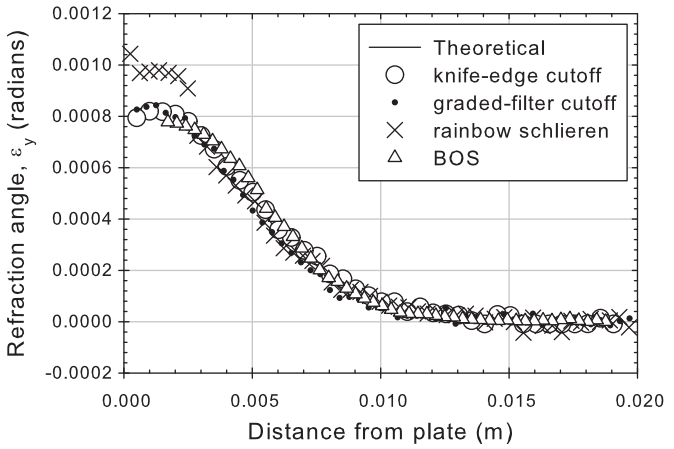


**Fig. 12.** Measured refraction angle versus distance from the heated plate for each of the quantitative schlieren techniques. The size of the round symbol for the knife-edge cutoff case is representative of the estimated error in each measurement.

## 5. Conclusions

As found earlier by Elsinga et al. [5], different schlieren techniques can easily make successful measurements of flow properties in two-dimensional refractive flows with accuracy in the $\pm$2–3% range. While their and our test cases were simple two-dimensional planar flows, others have also shown similar results for axisymmetric flows, where data processing must also include an Abel transform inversion [24,29] or related approach [35]. Since schlieren is an integrating optical method, its quantitative use in unknown three-dimensional flows requires a tomographic approach that is well beyond the present scope. The techniques described here are further limited to discontinuity-free flowfields (away from shock waves).

Both we and Elsinga et al. [5] used standard z-type parabolic-mirror schlieren instruments for quantitative measurements, the only additions being a means for calibration and the software required for data handling and analysis. These parallel-light systems (and also those based on high-quality lenses rather than mirrors) are best for quantitative schlieren of two-dimensional flows, and should be used wherever they are available. The utility of a graded-filter cutoff instead of a knife-edge in order to adjust the schlieren sensitivity and measurement range for a given application was already clear in qualitative imaging [1], and has been demonstrated here quantitatively.

An inexpensive and useful adjunct is Schardin's [4] long-focal-length calibration lens. Placed in an unused corner of the schlieren image, this lens provides a nearly automatic calibration of the schlieren system for quantitative studies.

The background-oriented schlieren technique (BOS), with non-parallel light passing through the flow under study, allows larger fields of view than traditional schlieren equipment. Also, in principle, only a suitable camera and background are required, aside from the digital-image-correlation software. BOS does not produce real-time schlieren images, and a correction is required for quantitative measurements in non-parallel light. Our results and those of Elsinga et al. [5] highlight the powerful importance of setting up BOS optics such that both the background and the flow under test are in razor-sharp focus. Beyond that, BOS is capable of producing quantitative data comparable to the data obtained using traditional schlieren instruments.

Rainbow schlieren suffered the most difficulties of the several methods we applied. Principally, while color transparency film is still available, the film developing process likely has a limited future. Rainbow schlieren provides few real benefits over the traditional monochrome knife-edge and graded-filter schlieren techniques that we applied, except for the provision of a colorful image that makes a qualitatively good flow illustration. Against this one must weigh the diffraction blurring that occurs when the rainbow transparency is used as a schlieren cutoff.

## References

[1] Settles GS. Schlieren and shadowgraph techniques: visualizing phenomena in transparent media. Springer-Verlag; 2001.
[2] Schmidt E. Schlierenaufnahmen des temperaturfeldes in der nahe wormeabgebender korper. Forschung auf dem Gebiete des Ingenieurwesens 1932;3(4):181–9.
[3] Schardin H. Das toeplersche schlierenverfahren: Grundlagen fur seine anwendung und quantitative auswertung. VDI-Forschungsheft No. 367 1934;5(4):1–32.
[4] Schardin H. Die schlierenverfahren und ihre anwendungen. Ergebnisse der Exakten Naturwissenschaften 1942;20:303–439.
[5] Elsinga GE, Oudheusden BWV, Scarano F, Watt DW. Assessment and application of quantitative schlieren methods: calibrated color schlieren and background oriented schlieren. Experiments in Fluids 2004;36(2):309–25.
[6] Meier GEA. Hintergrund schlierenmessverfahren. Deutsche Patentanmeldung; 1999.
[7] Dalziel SB, Hughes GO, Sutherland BR. Synthetic schlieren. In: Carlomagno GM, editor, Proc. 8th international symposium on flow visualization, vol. 62, Sorrento, Italy; 1998.
[8] Hooke R. Micrographia. London: J. Martyn and J. Allestry; 1665.
[9] Dalziel S, Hughes G, Sutherland B. Whole-field density measurements by 'synthetic schlieren'. Experiments in Fluids 2000;28(4):322–35.
[10] Raffel M, Richard H, Meier GEA. On the applicability of background oriented optical tomography for large scale aerodynamic investigations. Experiments in Fluids 2000;28(5):477–81.
[11] Richard H, Raffel M. Principle and applications of the background oriented schlieren (BOS) method. Measurement Science & Technology 2001;12(9):1576–85.
[12] Meier GEA. Computerized background-oriented schlieren. Experiments in Fluids 2002;33(1):181–7.
[13] Sutherland B, Flynn M, Onu K. Schlieren visualisation and measurement of axisymmetric disturbances. Nonlinear Processes in Geophysics 2003;10(3):303–9.
[14] Venkatakrishnan L, Meier GEA. Density measurements using the background oriented schlieren technique. Experiments in Fluids 2004;37(2):237–47.
[15] Yildirim B, Agrawal A. Full-field measurements of self-excited oscillations in momentum-dominated helium jets. Experiments in Fluids 2005;38(2):161–73.
[16] Goldhahn E, Seume J. The background oriented schlieren technique: sensitivity, accuracy, resolution and application to a three-dimensional density field. Experiments in Fluids 2007;43(2–3):241–9.
[17] Sommersel O, Bjerketvedt D, Christensen S, Krest O, Vaagsaether K. Application of background oriented schlieren for quantitative measurements of shock waves from explosions. Shock Waves 2008;18(4):291–7.
[18] Ihle C, Dalziel S, Nino Y. Simultaneous particle image velocimetry and synthetic schlieren measurements of an erupting thermal plume. Measurement Science and Technology 2009;20(12):125402 [5 p].
[19] Howes W. Rainbow schlieren. Technical Report TP-2166, NASA; 1983.
[20] Howes W. Rainbow schlieren and its applications. Applied Optics 1984;23(14):2449–60.
[21] Greenberg P, Klimek R, Buchele D. Quantitative rainbow schlieren deflectometry. Applied Optics 1995;34(19):3810–3.
[22] Agrawal A, Butuk N, Gollahalli S. Three-dimensional rainbow schlieren tomography of a temperature field in gas flows. Applied Optics 1998;37:479–85.
[23] Al-Ammar K, Agrawal A, Gollahalli S, Griffin D. Application of rainbow schlieren deflectometry for concentration measurements in an axisymmetric helium jet. Experiments in Fluids 1998;25(2):89–95.
[24] Agrawal A, Albers B, Griffin D. Abel inversion of deflectometric measurements in dynamic flows. Applied Optics 1999;38(15):3394–8.
[25] Agrawal A, Alammar K, Gollahalli S. Application of rainbow schlieren deflectometry to measure temperature and oxygen concentration in a laminar gas-jet diffusion flame. Experiments in Fluids 2002;32(6):689–91.
[26] Wong T, Agrawal AK. Quantitative measurements in an unsteady flame using high-speed rainbow schlieren deflectometry. Measurement Science & Technology 2006;17:1503–10.
[27] Satti R, Kolhe P, Olcmen S, Agrawal A. Miniature rainbow schlieren deflectometry system for quantitative measurements in microjets and flames. Applied Optics 2007;46(15):2954–62.
[28] Kolhe P, Agrawal A. Density measurements in a supersonic microjet using miniature rainbow schlieren deflectometry. AIAA Journal 2009;47(4):830–8.
[29] Kolhe P, Agrawal A. Abel inversion of deflectometric data: comparison of accuracy and noise propagation of existing techniques. Applied Optics 2009;48(20):3894–902.

[30] Tanda G, Devia F. Application of a schlieren technique to heat transfer measurements in free-convection. Experiments in Fluids 1998;24(4) 285–90.
[31] Ostrach S. An analysis of laminar free-convection flow and heat transfer about a flat plate parallel to the direction of the generating body force. Technical Report 2635, NACA; 1952.
[32] Gonzalez RC, Woods RE. Digital image processing. Upper Saddle River, New Jersey, USA: Prentice-Hall; 2002.
[33] Hargather MJ, Settles GS. Natural-background-oriented schlieren. Experiments in Fluids 2010;48(1):59–68.
[34] Hargather MJ, Lawson MJ, Settles GS, Weinstein LM. Seedless velocimetry measurements by schlieren image velocimetry. AIAA Journal 2011;49(3): 611–20.
[35] Venkatakrishnan L. Density measurements in an axisymmetric underexpanded jet by background-oriented schlieren technique. AIAA Journal 2005;43:1574–9.